ACS OMEGA

http://pubs.acs.org/journal/acsodf

Article

Chemical Emissions from Cured and Uncured 3D-Printed Ventilator Patient Circuit Medical Parts

Jordan E. Krechmer,* Brennan Phillips, Nicholas Chaloux, Russell Shomberg, Conner Daube, Gaurav Manchanda, Sam Murray, Alex McCarthy, Rodrigo Fonseca, Jinen Thakkar, Brice Loose, Scott C. Herndon, John T. Jayne, Douglas R. Worsnop, and Manjula R. Canagaratna

Cite This: *ACS Omega* 2021, 6, 30726−30733

Read Online

ACCESS | Metrics & More | Article Recommendations | Supporting Information

ABSTRACT: Medical shortages during the COVID-19 pandemic saw numerous efforts to 3D print personal protective equipment and treatment supplies. There is, however, little research on the potential biocompatibility of 3D-printed parts using typical polymeric resins as pertaining to volatile organic compounds (VOCs), which have specific relevance for respiratory circuit equipment. Here, we measured VOCs emitted from freshly printed stereolithography (SLA) replacement medical parts using proton transfer reaction mass spectrometry and infrared differential absorption spectroscopy, and particulates using a scanning mobility particle sizer. We observed emission factors for individual VOCs ranging from ∼0.001 to ∼10 ng cm^{-3} min^{-1}. Emissions were heavily dependent on postprint curing and mildly dependent on the type of SLA resin. Curing reduced the emission of all observed chemicals, and no compounds exceeded the recommended dose of 360 μg/d. VOC emissions steadily decreased for all parts over time, with an average *e*-folding time scale (time to decrease to $1/e$ of the starting value) of 2.6 ± 0.9 h.

1. INTRODUCTION

The coronavirus disease 2019 (COVID-19) pandemic created shortages of critical medical equipment such as ventilators, personal protective equipment (PPE) including masks and face shields and diagnostic supplies such as nasal swabs.[1,2] This shortage was caused by a simultaneous increase in demand of medical supplies as the number of COVID patients increased, and a reduction in supply due to large disruptions of production and delivery supply chains. While many producers of PPE and medical devices drastically scaled up production, some hospitals, governments, and nonprofits used additive manufacturing (AM), or three-dimensional (3D) printing, to build parts or medical equipment.[3,4]

3D printing describes a general process in which a printer builds an object by selectively adding or curing a material following a preprogrammed design. There are several different types of 3D-printing processes used in a variety of applications, and each technique has distinct advantages and disadvantages. A few of the most popular AM methods include, but are not limited to, material extrusion, vat photopolymerization, material jetting (also called inkjet printing), and powder bed fusion. In material extrusion, a polymer or wax is heated and then extruded by a nozzle to deposit layers to build a part. Material extrusion is fast and relatively low-cost, but parts made by some technological variations such as fused filament fabrication ("3D") printing can be of relatively low quality and is typically used for gadgets or prototyping.[5] Inkjet printing is typically used to produce high-quality parts from light-curing liquid resins; depending on the intended properties of the printed part, the resin can contain additives such as ceramics. The liquid is deposited as a droplet in layers to form a part, and inkjet printers can control different printing variables by altering droplet properties. Powder bed fusion uses a laser or other high energy sources to fuse successive layers of fine powder. Once the part is finished, a vacuum removes excess powder.[6]

This work only examines parts printed using vat photopolymerization, specifically stereolithography (SLA), which is distinguished as a technique by using ultraviolet (UV) light to produce parts from light-curing liquid resins. SLA is popular for biomedical applications because of the high quality and resolution (down to 10 μm) of printed parts, though it is expensive and relatively time-consuming compared to other methods. During the SLA polymer-printing process, a liquid resin is cross-linked into a solid polymer using a photochemical reaction. Excess uncured resin is washed away with a solvent, typically isopropyl alcohol though other solvents may be used, and then optional additional curing is completed by exposing the part to heat and UV light. While 3D printing usually takes longer to produce objects per part than many mass production methods such as injection molding, 3D printers themselves exist in large quantities and have the flexibility to print parts in a variety of shapes and designs that can be difficult to

Received: August 27, 2021
Accepted: October 22, 2021
Published: November 8, 2021

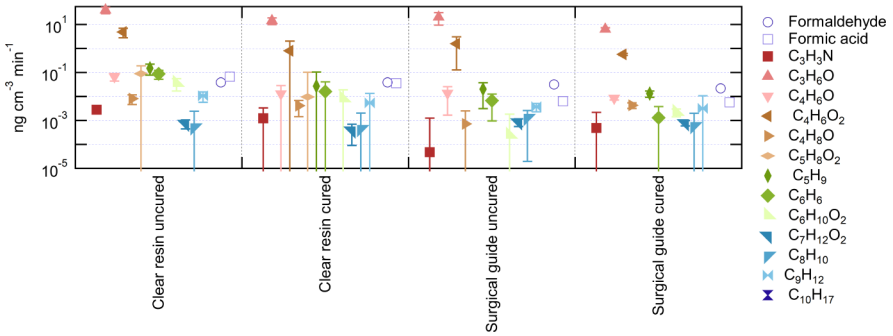

Figure 1. Emission factors in units of nanograms per cubic centimeter (cm^3) per minute for mass spectral signals measured using a Vocus proton transfer reaction-time-of-flight spectrometer and formic acid and formaldehyde measured using a tunable infrared differential absorption spectrometer. Error bars represent the standard error of the mean (SEM) of multiple measurements. The tunable infrared differential absorption spectrometer only made one set of measurements, so formic acid and formaldehyde are presented without error bars.

manufacture with traditional methods. 3D printing also does not require expensive retooling to produce a new part or design. A user can download a structural design file from another user and print the same part on a printer in an entirely different location. 3D printers employ a variety of materials and techniques, depending on the application and manufacturer. Because they are lightweight, easily sterilized, and low-cost, most replacement medical parts for the applications mentioned above are printed or molded from polymer plastics.[6] Certain types of printers and materials, including SLA/resin printers, are particularly suited for sealed hydraulic and pneumatic applications due to their ability to print with 100% infill and with sufficiently high resolution to completely seal gaskets, O-rings, compression fittings, and sealed threads.

3D-printed polymer-based parts are increasingly used in various medical equipment and consumer products, where emissions from the printed part could present a health hazard or nuisance odors. Before the COVID-19 pandemic, researchers explored the use of 3D-printed respirators for applications such as better fitting face masks[7−9] or medical implants,[10] but this research rapidly accelerated from 2020 to 2021.[4,11,12] Additionally, 3D-printed parts are now frequently used in sensitive analytical instrumentation.[13,14] some of which are designed to measure pollutants that the parts themselves could emit.[15] Uncharacterized emissions could potentially induce error, bias, or artifacts into measurements made with 3D-printed parts.

There is relatively little literature on the composition of toxic chemicals that affect biocompatibility of 3D-printed parts with living organisms, as well as the toxicity of finished 3D-printed parts. Unprocessed or uncured liquid resins are often toxic, and Oskui et al.[16] reported that uncured 3D-printed parts killed zebrafish. However, curing the parts after printing reduced emissions to the point where zebrafish were healthy enough to perform experiments with the 3D-printed substrate. Similarly, MacDonald et al. suggested to use zebrafish embryos as a diagnostic assay for biocompatibility.[17] Other literature has demonstrated that 3D-printed polymers are potential endocrine disrupters in embryos, particularly those leaching diethyl phthalate polyethylene glycol.[18] Additional research groups have evaluated 3D-printed parts on different biological matrices,[18−21] particularly for dental applications.[22] Several of these studies reported that curing or postprocessing with heat reduced toxicity.[17,20,23] Other studies showed that solvent-based washes could eliminate toxic byproducts, such as supercritical CO_2 used by Popov et al.,[24] to remove monomers from 3D-printed cranial implants or isopropyl alcohol by Xu et al. for dental implants.[25] Few studies even attempt to explicitly identify the molecular composition of the toxic compounds and none evaluate the biological safety effects of the 3D-printed parts on a breathing gas pathway.

Researchers have extensively studied both particulate and gaseous emissions produced directly from 3D printers during the printing process[26−28] with a focus on ultrafine particle emissions,[29,30] and there are many additional studies examining emissions from other polymeric processes (e.g., plastic recycling in Unwin et al.[31]). Of particular relevance for this work, Väisänen et al.[32] measured gas-phase volatile organic compound (VOC) emissions during the printing process of an SLA Formlabs printer and detected several different compounds in excess of the background. There are, however, no published studies directly characterizing particulate and gaseous emissions from the finished printed parts. Most of the 3D-printed parts are used for consumer-facing applications (with exceptions for dental implants and some other applications noted above), for which there are no testing regimes or regulations. This enables 3D-printed PPE such as masks or face shields to be used without prior testing. The ventilator parts used in this study, however, are medical devices and would be subject to strict regulatory testing requirements before use just as medical devices produced from traditional manufacturing methods.

The International Organization for Standardization (ISO) has issued a series of protocols, ISO-18562-3:2017, for testing of VOCs emitted from breathing apparatuses, and ISO-18562-2:2017, for testing of particulate emissions. Typically, testers would use a thermal desorption gas chromatograph to measure VOC concentrations from parts 3 times over a 24 h period. If the identified VOC does not have an established tolerable intake (TI) level, then the standard has varying levels of toxicological thresholds of concern (TTC) ranging from 40 μg per day for long term exposure devices (used for >30 days) to 360 μg per day per chemical constituent for short duration devices (used for <24 h).[33]

In this work, we use three different analytical instruments to measure gas- and condensed-phase (particulate) emissions from recently printed substitute medical parts. Largescale production of these 3D parts was a potential course of action to mitigate the surge of COVID patients expected to outpace the supply of ventilators. Here, we focus on two types of 3D-printed parts for emergency pulmonary care: (1) flow splitters to split one ventilator to two patients;[34] and (2) an oxygen

https://doi.org/10.1021/acsomega.1c04695
ACS Omega 2021, 6, 30726−30733

enrichment port used to increase the proportion of oxygen in a ventilator or a continuous positive air pressure (CPAP) or bilevel positive air pressure device (BiPAP). We performed these measurements to better characterize the composition and concentrations of gas and particle species emitted by 3D parts in real-time under conditions that simulate use scenarios. Rather than use a more-typical gas chromatograph that provides discrete sampling over 20−60 min time intervals, we performed real-time measurements using an online chemical ionization mass spectrometer acquiring an entire mass spectrum per second over long periods (either 5 min or 10 h) for all measured parts. While the time-of-flight mass spectrometer (TOF-MS) does not provide unambiguous structural identification as gas chromatography (GC)−MS does, we obtain a time-resolved picture of the emission process. Thus, we were able to measure some parts over a continuous multihour period to observe the full off gassing and equilibration process. To the best of our knowledge, these are the first published measurements of gas and aerosol emissions directly from cured and uncured 3D-printed parts.

2. RESULTS AND DISCUSSION

2.1. Emission Factors. Figure 1 shows calculated emission factors for common VOCs from four different types of 3D-printed parts, photos of which we present in Figure S1. We present emissions from two parts printed in Formlabs clear resin (FLGPCL02, Formlabs), with one part cured and one not cured. We also show emissions from two parts printed out of Formlabs surgical guide resin, (FLSGAM01, Formlabs) with one cured and one uncured (see the Methods section for a more thorough definition of the curing process). Both resins are acrylate-based. The surgical guide resin (Formlabs, Somerville, MA, USA) is intended for 3D-printed endosseous dental implant accessories such as dental surgical guides. Figure 1 presents emissions in units of nanograms per cubic centimeter per minute (ng cm^{-3} min^{-1}), so that emission factors may be scalable to the relevant total surface area of printed parts for evaluating other 3D-printed parts or to use in exposure models. Each mass spectral measurement in Figure 1 is the average of three discrete measurements of three different copies of the same part. The error bars represent the standard error of the mean.

The Figure 1 legend lists signals differently depending on the method of detection. The legend explicitly lists formic acid (HCOOH) and formaldehyde (HCHO) by name because they were unambiguously identified using infrared spectroscopy. We list mass spectral measurements as elemental formulas because a time-of-flight mass spectrometer cannot distinguish structural isomers. While the time-of-flight mass spectrometer enables the simultaneous measurement of hundreds of ions every second, we choose to focus our analysis on specific analytes using two criteria: first, prior inference that is based on the expected chemical composition of the resin and associated byproducts emitted during curing. Second, we identify ions that increase when comparing the mass spectra between zero air backgrounds and sampling of 3D-printed parts. Because the clear resin is composed of methacrylated oligomers and monomers that are bonded together during the printing process, we targeted measurements of likely residual trace volatiles such as $C_4H_6O_2$ (methyl acrylate), $C_5H_8O_2$ (methyl methacrylate), $C_6H_{10}O_2$ (ethyl methacrylate), and $C_7H_{12}O_2$ (propyl methacrylate). In the uncured resins, we do observe elevated values of $C_4H_6O_2$ (likely methyl acrylate) and $C_5H_8O_2$ (methyl methacrylate). Both signals decrease significantly after curing. While acrylonitrile-butadiene-styrene (ABS) polymer is a commonly used solid plastic feedstock for material extrusion, Formlabs printers cannot use it as the liquid resin used to produce printed parts, nor are the printers themselves constructed from ABS. The parts were handled with nitrile gloves, however, so we hypothesize that the C_3H_3N signal (acrylonitrile) could be contamination from handling. Thus, we also report emission factors for acrylonitrile, which is low compared to the other emissions and has no appreciable decrease with curing within the error bars of the measurement. We also include additional signals such as C_6H_6 (benzene), C_8H_{10} (xylenes), C_9H_{12} (trimethyl benzene/ethyl benzene/ethyl toluene/propyl benzene), C_5H_8 (cyclopentene/isoprene), and $C_{10}H_{16}$ (monoterpenes or other petroleum-derivative alkenes).[35] Table S1 of the Supporting Information lists the likely and possible molecules for each of the formulas. In the text, we refer to both for clarity.

Many of the compounds we detected were also reported by Väisänen et al.,[34] who measured emissions using GC−MS from various printers, including a Formlabs SLA printer. The two compounds they detected in the highest abundance were methyl methacrylate and ethyl methacrylate, which we also observed with a proton transfer reaction mass spectrometer in high quantities directly from the part. They detected a small amount of benzene above the background, which we also interestingly measured from the printed part, but could not explain the origin of. Their measurement suggests that the benzene or some other compounds could have adsorbed to or absorbed into the part during the printing process. They did not detect siloxanes, which we also failed to measure. They did detect acetic acid during the middle of the printing process, but not at the end. Thus, the lack of acetic acid in our measurements of the finished part is consistent, otherwise Väisänen et al. likely would have measured some at the end of the printing process. In general, we find our measurements to be consistent with those in Väisänen et al., and useful to confirm which chemicals they observed came from the part or resin itself (esters) or from the printing process (acetic acid).

Figure S2 shows the same measurements in Figure 1, but in units of μg/d and plotted with the limit listed in the ISO protocol of 360 μg/d. All signals, except for C_3H_6O (acetone/propanal) for the clear resin and uncured surgical guide resin, are below this threshold. All measured signals for the cured surgical guide are below the threshold. Most of the reported signals are considerably lower than the daily threshold, by 2 or 3 orders of magnitude.

While the surgical guide resin has lower emissions than the clear resin, Figure 1 shows that curing has a much larger effect on emission levels than the choice of resin. For both the clear resin and the surgical guide resin, curing reduces the emission factors for all measured signals and compounds, in some cases up to a factor of 10× less. Emissions from the cured clear resin are comparable to those from the cured surgical guide resin.

We also tested a second set of parts printed from other types of resins and different cures, printed by the same Formlabs SLA printer. We present more details on these parts and the printer in Section 3.1. This second set of experiments was semiquantitative because we did not accurately measure the dilution flow or take replicate measurements to gauge precision and reproducibility. The experimental conditions were consistent, however, and enable qualitative comparisons of different resins against one another. In Figure S3, we show

https://doi.org/10.1021/acsomega.1c04695
ACS Omega 2021, 6, 30726−30733

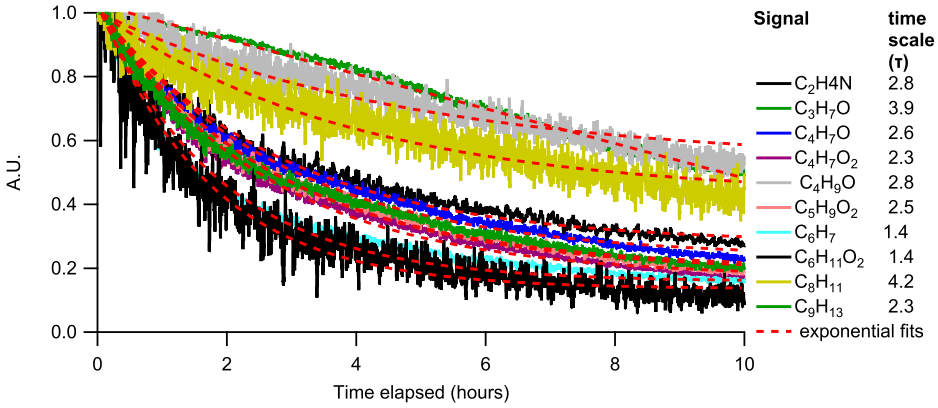

Figure 2. Emission trends for selected analytes over a 10 h period of continuous air flow. The emission currents were fit with an exponential decay function to estimate their *e*-folding emissions time.

emission factors for additional curing and resin types that have similar trends to Figure 1. Figure S3 has measurements from an uncured part, a part cured for only 20 min, and a part cured for only 60 min. The more curing, the more emissions decrease for almost all the signals shown. In these sets of experiments, ethanol is very high, which we hypothesize is residue from cleaning the parts after printing.

Overall, our gas-phase measurements from both experimental sets clearly show that curing is effective in reducing the emissions of VOCs from 3D-printed parts, regardless of the resin type. This is consistent with some of the previous reports in the literature, which measured an increase in biocompatibility after curing.[16,23]

In addition to the gaseous emission measurements in Figure 1, we also present particulate emission measurements in Figure S4 obtained using a scanning mobility particle sizer. For the four different resins sampled in Figure 1, we detect no particulate emissions from measurements of the particle number concentration (number/cm^3), particle volume, or particle area. This is expected, as the parts do not have dust or loose material that could be resuspended, and the emissions of low volatility gases capable of nucleation would be extremely low at room temperature.

2.2. Time-Dependent Decay of Emissions. In addition to the emission factor measurements, we evaluated a single printed part to determine its emission time scale over a period of several hours. Air was continuously flushed over the part and brought to the instrument for analysis. In contrast to the ISO testing protocol, which only requires GC−MS point measurements three times in a 24 h period, with the online proton transfer reaction mass spectrometer we were able to take a measurement every second and observe temporal trends in emissions. Figure 2 shows an approximately 10 h long time series of the same mass spectral signals in Figure 1. All the signals are normalized to their max intensity for easy comparison. The signals are plotted with an exponential decay determined from a least-squares fit of the measurement trace to the following equation

$$y(t) = y_0 \exp\left(-\frac{t - t_0}{\tau_d}\right) \quad (1)$$

where t_0 is the time of the peak in the compound concentration, y_0 is the peak value of y, and τ is the timescale of the decay to equilibrium.

Over the first 10 h of the measurement, the reported compounds decrease with *e*-folding time scales ranging from 1.4 to 4.2 h, and with an average *e*-folding decay of 2.6 ± 0.9 h.

While we have not found any examples in the literature of direct part emission measurements over time, other groups have used biological proxies to measure the diminishing effect of emissions. Notably, Inoue and Ikuta[23] heated 3D-printed parts, including SLA parts from Formlabs printers, and extracted gaseous emissions in a water trap. Absorbance spectra suggested that the VOC bulk with an absorbance peak at 245 nm decreases by an *e*-folding time scale of less than 1 h. This is slightly faster than our results by a factor of ∼2× of 3×, but there are many uncertainties in comparing speciated mass spectral signals with bulk 245 nm absorbance spectra. Most obviously, Inoue and Ikuta did not know exactly which compounds were absorbing at 245 nm and had no clues as to the functionality or vapor pressure. Furthermore, some chemical transformation—possibly oxidation—occurred during Inoue and Ikuta's curing process because they report that the clear parts turned brown after curing in both air and N_2 (though somewhat less so in N_2).

We suggest that the approach in this manuscript is easier to implement than other more sophisticated and effective methods such as washing with supercritical CO_2.[24] While it totally eliminates byproducts, supercritical CO_2 requires relatively expensive and specialized materials but leaving the part out under a clean buffer gas is achievable in almost any laboratory or maker space. Additional washing with solvents, such as ethanol or isopropyl alcohol, also has shown to increase biocompatibility in cell cultures or zebrafish.[17,25] The esters (e.g., methyl methacrylate) are likely soluble in alcohol solvents and will be effective in washing them away. However, we note that our parts were washed with isopropyl alcohol after finishing and we still detected numerous emissions in our tests.

The decay times suggest that, in addition to, or in place of, curing for 30 min or longer, leaving the parts in a ventilated area for 2−3 h (kept sterile for medical equipment) would significantly (by a factor of *e*) reduce the magnitude of VOC emissions. This is consistent with prior results that suggest that biocompatibility can be improved on a similar time scale.[23] Keeping the part at an elevated temperature would increase the rate of outgassing and can reduce harmful VOCs present before use in a medical or other consumer setting. Additionally, emission tests for regulatory purposes should be completed with the part maintained at a constant temperature.

https://doi.org/10.1021/acsomega.1c04695
ACS Omega 2021, 6, 30726−30733

3. METHODS

3.1. 3D-Printed Parts. We performed two separate sets of experiments sampling two different sets of 3D-printed parts. Set 1 contained three different types of resins and two different types of cures, but the sampling protocol was not quantitative and could not be used to produce accurate absolute emission factors. Thus, we present relative emission factors of the parts in arbitrary units relative to one another in Figure S3. To measure more quantitatively accurate absolute emission factors, we performed a more focused second set of experiments (set 2) with a quantitative sampling system but sampled only two parts and two cure types (cured and uncured).

We printed and tested emissions from flow splitters, used to share ventilators,[34,36] and oxygen enrichment ports that were produced in a laboratory at the University of Rhode Island using Formlabs Form 2 SLA 3D printers. Figure S1 shows photographs of the printed parts we used for testing. During the printing process, uncured liquid photopolymer resin is cross-linked into solid polymer using a laser-driven photochemical reaction. Excess uncured resin is then washed away with >90% isopropyl alcohol.

Curing, a post processing step, included exposing the part to 405 nm light from all directions and heating the part to 60 C for a 30 min cycle using a Formlabs cure unit. In Set 1, we tested parts that were cured for either 20 or 60 min. After printing and curing, we placed each part into a small plastic bag, sealed it, and transported the parts by vehicle from the University of Rhode Island in Narragansett, RI, USA to Aerodyne Research in Billerica, MA, USA for measurements. For set 1, the age of the parts at the beginning of testing at Aerodyne was 8 to 12 h, but because they were sealed in small plastic bags, we assume outgassing was limited. The age of the parts for set 2 was approximately 24 h. Both timelines mimic a theoretically realistic manufacturing and logistics process that includes printing, delivering, and deploying 3D-printed medical parts in a clinical or consumer setting, and should represent an upper bound on emissions. Longer storage times would theoretically reduce emissions.

3.2. Analytical Instrumentation. To measure VOCs, we used a Vocus 2R proton transfer time-of-flight mass spectrometer (Tofwerk, AG, Thun, Switzerland). PTR-TOF is a chemical ionization MS technique in which hydronium (H_3O^+) ions transfer a proton to any neutral molecule with a proton affinity higher than that of water.[37] The Vocus proton transfer time-of-flight mass spectrometer is a novel PTR source in which the traditional PTR drift tube is replaced with a focusing ion-molecule reaction region (fIMR) surrounded by a quadrupole that focuses the ions along the central axis resulting in a large increase in sensitivity[38] and faster response times due to no analyte contact with metal parts.[39] It can efficiently sample both VOCs and oxygenated VOCs (oVOCs).[40] In this experiment, the instrument had a mass resolving power of ~10,000 m/dm at m/z 107.

We calibrated the Vocus proton transfer time-of-flight mass spectrometer by diluting and injecting common VOCs from a preprepared standard tank (Apel-Riemer Environmental, Miami, FL, USA) into the instrument. The standard mix contained volatile chemicals common to the Earth's atmosphere and was not designed specifically to measure emissions from 3D-printed parts. Thus, to calibrate additional observed signals, we estimated the kinetic proton capture rate coefficient using a published formulation for the dipole moment and polarizability of the molecule. We calculated sensitivity from the estimated rate coefficient by computing a regression of compounds that we explicitly calibrated using the calibration mixture (Figure S5). We note that this method has an approximately 50% uncertainty, which should be considered when using the emission factors from this study.[41,42]

We measured suspended particulates, or aerosols, with a scanning mobility particle sizer (TSI Inc.) consisting of a condensation particle counter (CPC; model 3776; TSI Inc, MN, USA) and a differential mobility analyzer (DMA; model 3081; TSI Inc., MN, USA). The scanning mobility particle sizer scanned for particulates from 14.6 to 532 nm over a scan duration of 120 s and then ramped back down for 15 s, resulting in a 135 s measurement time resolution.

We used a tunable infrared differential absorption spectrometer[43] to measure formaldehyde (HCOH) and formic acid (HCOOH). Details of the instrument and its configuration have been described in depth in previous literature.[44]

We only used the Vocus proton transfer time-of-flight mass spectrometer for the set 1 experiments that provide qualitative measurements of curing types. In set 2 experiments, we measured with the Vocus proton transfer time-of-flight mass spectrometer, scanning mobility particle sizer, and tunable infrared differential absorption spectrometer to obtain quantitative measurements of emission factors.

3.3. Sampling Procedure. For Vocus proton transfer time-of-flight mass spectrometer measurements of gas-phase emissions, we placed a single part at a time into a small (~1 L) custom-constructed fluorinated ethylene propylene (FEP) Teflon bag and sealed the bag with a Teflon FEP panel taped to the outside of the bag with a special VOC-free adhesive tape that can stick to teflon surfaces (3M Corp.). The FEP bags are popular for use in atmospheric chemistry experiments because their surfaces are chemically inert, do not serve as catalysts, and have minimal gas−wall interactions compared to other materials.[45,46] The Vocus proton transfer time-of-flight mass spectrometer sampled from the part-containing bag at a flow rate of 1.0 SLPM and the tunable infrared differential absorption spectrometer at 0.5 SLPM (when in use). Both instruments drew sample air via a 1/4″ OD perfluoroalkoxy alkane line. The line to the proton transfer time-of-flight mass spectrometer was 0.3 m long, and the line to the tunable infrared differential absorption spectrometer was ~15 m long because the instrument was in an adjacent laboratory room. The total flow into the bag was 2.5 SLPM, and the excess was blown off from an open valve on the sampling outlet to ensure the sampling bag was at a slight positive pressure, and that there were no leaks of room air into the bag, part, or sampling orifice. We corrected the measured concentrations for the 1:2.5 dilution ratio in data postprocessing. As a sample carrier gas, we flowed clean synthetic air that was made from the gaseous blowoff of a liquid nitrogen (N_2) dewar and liquid oxygen (O_2) dewar together into a 20% oxygen mix.

For scanning mobility particle sizer measurements, we used a metal sampling apparatus to reduce losses of charged particles to surfaces. We placed a single part at a time into a sealable stainless-steel container, locked with a stainless-steel vacuum flange and a Viton gasket. The synthetic clean air flowed into the container through a 1/4″ Swagelok fitting, pushing sample air over the part and into a 1/4″ OD copper line to the scanning mobility particle sizer.

https://doi.org/10.1021/acsomega.1c04695
ACS Omega 2021, 6, 30726−30733

We recorded blanks or background measurements by flowing synthetic air through each container before measuring each part. The value of the background was subtracted in postprocessing and the data in both Figures 1 and 2 are background-corrected.

3.4. Emission Factor Calculations. To determine an individual VOC emission factor for each part in units of ng cm^{-3} min^{-1}, as in Figure 1, we first converted the calibrated gas-phase steady-state concentration [C] of the VOC in units of parts-per-billion by volume (ppbv) to an emission factor, EF, in units of $\mu g\ m^{-3}$

$$\mathrm{EF}\ (\mu g/m^3) = \frac{[C] \times MW \times 0.0409 \times F_L}{SA} \quad (2)$$

where MW is the molecular weight of the detected ion in units of g/mol. We used the molecular weight of the ion minus one hydrogen atom (−H), to account for the proton added during ionization. At 1 atm and 25 °C, air contains 4.09×10^{-2} mol L^{-1}. Adjusting units of mol L^{-1} to $\mu g\ m^{-3}$ results in a factor of $(0.0409 \times MW)$ to convert calibrated signals in units of ppbv into $\mu g\ m^{-3}$. We then normalize to the surface area ratio, SA, of the parts, for which the flow splitter had a total area of 5633 mm^2 and the oxygen enrichment port had a total surface area of 3071 mm^2. Our total flow into the measurement bag was 2.5 SLPM, which we multiply by (F_L) to obtain emissions on a per-minute basis.

For the emission factors reported in dose units in Figure S2, we converted measured concentrations from units of ppbv to $\mu g\ day^{-1}$ using the following formula.

$$\mathrm{EF}\ (\mu g/m^3) = \frac{[C] \times MW \times 0.0409 \times D \times BR[\times 0.54]}{2} \quad (3)$$

D accounts for the 1:2.5 dilution in the total flow versus the flow sampled by the tunable infrared differential absorption spectrometer, scanning mobility particle sizer, or Vocus proton transfer time-of-flight mass spectrometer. BR normalizes the concentration to the average breath per adult human per day of 20 $m^3\ day^{-1}$.[33] The sampling setup results in a measurement of emissions from the surface of the entire part, but in a real-world use case, only emissions from the inside surface of the part would be exposed to human lungs. To account for this, we assume the inside and outside surface areas are symmetric and we divide the emission factor by 2, given that the parts are almost completely symmetric between the inside and outside. Finally, emission factors for the flow splitters were multiplied by a factor of 0.54 to normalize emissions to those of an oxygen enrichment port (3071:5633 mm^2).

■ ASSOCIATED CONTENT

Supporting Information

The Supporting Information is available free of charge at https://pubs.acs.org/doi/10.1021/acsomega.1c04695.

Part photographs; additional emission factor plots; Vocus proton transfer time-of-flight mass spectrometer calibration information; and likely molecular identifications for mass spectral signals(PDF)

■ AUTHOR INFORMATION

Corresponding Author

Jordan E. Krechmer − *Aerodyne Research, Inc., Billerica, Massachusetts 01821, United States;* orcid.org/0000-0003-3642-0659; Phone: 978 633-9500; Email: krechmer@aerodyne.com

Authors

Brennan Phillips − *Department of Ocean Engineering, The University of Rhode Island, Narragansett, Rhode Island 02882, United States*

Nicholas Chaloux − *Department of Ocean Engineering, The University of Rhode Island, Narragansett, Rhode Island 02882, United States*

Russell Shomberg − *Department of Ocean Engineering, The University of Rhode Island, Narragansett, Rhode Island 02882, United States*

Conner Daube − *Aerodyne Research, Inc., Billerica, Massachusetts 01821, United States*

Gaurav Manchanda − *Formlabs, Inc., Somerville, Massachusetts 02143, United States*

Sam Murray − *Formlabs, Inc., Somerville, Massachusetts 02143, United States*

Alex McCarthy − *Formlabs, Inc., Somerville, Massachusetts 02143, United States*

Rodrigo Fonseca − *Computer Science Department, Brown University, Providence, Rhode Island 02903, United States;* Present Address: Principal Researcher, Microsoft Research, Redmond, WA 98052 US

Jinen Thakkar − *Department of Medicine, Brown University and Alpert Medical School, Providence, Rhode Island 02903, United States*

Brice Loose − *Department of Ocean Engineering, The University of Rhode Island, Narragansett, Rhode Island 02882, United States*

Scott C. Herndon − *Aerodyne Research, Inc., Billerica, Massachusetts 01821, United States*

John T. Jayne − *Aerodyne Research, Inc., Billerica, Massachusetts 01821, United States*

Douglas R. Worsnop − *Aerodyne Research, Inc., Billerica, Massachusetts 01821, United States*

Manjula R. Canagaratna − *Aerodyne Research, Inc., Billerica, Massachusetts 01821, United States*

Complete contact information is available at: https://pubs.acs.org/10.1021/acsomega.1c04695

Author Contributions

J.E.K., M.R.C., N.C., and C.D. conducted measurements and took data. B.P., R.S., A.C., S.M., R.F., J.T., and B.L. designed and printed 3D parts for analysis. J.T.J., D.T.W., S.C.H., B.L. and G.M. provided input on experimental design. J.E.K., B.P., and S.M. wrote the manuscript. All authors edited and contribued to the manuscript text.

Notes

The authors declare the following competing financial interest(s): JEK, MRC, CD, SH, JTJ, DRW are employees of Aerodyne Research, Inc., which commercializes the Vocus for geoscience research. SM, GM, and AM are employees of Formlabs, which designs, manufactures, and sells the 3D printers and resin materials used in this study.

■ ACKNOWLEDGMENTS

We are grateful to Professor Brian Heikes of the University of Rhode Island for bringing several diverse groups together and making this work possible. No external funding is acknowledged.

REFERENCES

(1) Livingston, E.; Desai, A.; Berkwits, M. Sourcing Personal Protective Equipment During the COVID-19 Pandemic. *JAMA, J. Am. Med. Assoc.* **2020**, *323*, 1912.

(2) Vermeiren, C.; Marchand-Senécal, X.; Sheldrake, E.; Bulir, D.; Smieja, M.; Chong, S.; Forbes, J. D.; Katz, K. Comparison of Copan ESwab and FLOQSwab for COVID-19 Diagnosis: Working around a Supply Shortage. *J. Clin. Microbiol.* **2020**, *58*, 19−20.

(3) Tino, R.; Moore, R.; Antoline, S.; Ravi, P.; Wake, N.; Ionita, C. N.; Morris, J. M.; Decker, S. J.; Sheikh, A.; Rybicki, F. J.; Chepelev, L. L. COVID-19 and the Role of 3D Printing in Medicine. *3D Print. Med* **2020**, *6*, 11.

(4) Ishack, S.; Lipner, S. R. Applications of 3D Printing Technology to Address COVID-19−Related Supply Shortages. *Am. J. Med.* **2020**, *133*, 771−773.

(5) Mohamed, O. A.; Masood, S. H.; Bhowmik, J. L. Optimization of Fused Deposition Modeling Process Parameters: A Review of Current Research and Future Prospects. *Adv. Manuf.* **2015**, *3*, 42−53.

(6) Ngo, T. D.; Kashani, A.; Imbalzano, G.; Nguyen, K. T. Q.; Hui, D. Additive Manufacturing (3D Printing): A Review of Materials, Methods, Applications and Challenges. *Composites, Part B* **2018**, *143*, 172−196.

(7) Han, D. H.; Rhi, J.; Lee, J. Development of Prototypes of Half-Mask Facepieces for Koreans Using the 3D Digitizing Design Method: A Pilot Study. *Ann. Occup. Hyg.* **2004**, *48*, 707−714.

(8) Cai, M.; Li, H.; Shen, S.; Wang, Y.; Yang, Q. Customized Design and 3D Printing of Face Seal for an N95 Filtering Facepiece Respirator. *J. Occup. Environ. Hyg.* **2018**, *15*, 226−234.

(9) Joe, P. S.; Shum, P. C.; Brown, D. W.; Lungu, C. T. A Novel Method for Designing and Fabricating Low-Cost Facepiece Prototypes. *J. Occup. Environ. Hyg.* **2014**, *11*, 665−671.

(10) Tappa, K.; Jammalamadaka, U. Novel Biomaterials Used in Medical 3D Printing Techniques. *J. Funct. Biomater.* **2018**, *9*, 17.

(11) Tong, Y.; Pan, J.; Kucukdeger, E.; Johnson, A. L.; Marr, L. C.; Johnson, B. N. 3D Printed Mask Frames Improve the Inward Protection Efficiency of a Cloth Mask. *ACS ES&T Engg* **2021**, *1*, 1000−1008.

(12) Zimmerling, A.; Chen, X. Innovation and Possible Long-Term Impact Driven by COVID-19: Manufacturing, Personal Protective Equipment and Digital Technologies. *Technol. Soc.* **2021**, *65*, 101541.

(13) Salentijn, G. I.; Permentier, H. P.; Verpoorte, E. 3D-Printed Paper Spray Ionization Cartridge with Fast Wetting and Continuous Solvent Supply Features. *Anal. Chem.* **2014**, *86*, 11657−11665.

(14) Yang, Y.; Liu, H.; Chen, Z.; Wu, T.; Jiang, Z.; Tong, L.; Tang, B. A Simple 3D-Printed Enzyme Reactor Paper Spray Mass Spectrometry Platform for Detecting BuChE Activity in Human Serum. *Anal. Chem.* **2019**, *91*, 12874−12881.

(15) Cross, E. S.; Williams, L. R.; Lewis, D. K.; Magoon, G. R.; Onasch, T. B.; Kaminsky, M. L.; Worsnop, D. R.; Jayne, J. T. Use of Electrochemical Sensors for Measurement of Air Pollution: Correcting Interference Response and Validating Measurements. *Atmos. Meas. Tech.* **2017**, *10*, 3575−3588.

(16) Oskui, S. M.; Diamante, G.; Liao, C.; Shi, W.; Gan, J.; Schlenk, D.; Grover, W. H. Assessing and Reducing the Toxicity of 3D-Printed Parts. *Environ. Sci. Technol. Lett.* **2016**, *3*, 1−6.

(17) MacDonald, N. P.; Zhu, F.; Hall, C. J.; Reboud, J.; Crosier, P. S.; Patton, E. E.; Wlodkowic, D.; Cooper, J. M. Assessment of Biocompatibility of 3D Printed Photopolymers Using Zebrafish Embryo Toxicity Assays. *Lab Chip* **2016**, *16*, 291−297.

(18) De Almeida Monteiro Melo Ferraz, M.; Henning, H. H. W.; Ferreira da Costa, P.; Malda, J.; Le Gac, S.; Bray, F.; Van Duursen, M. B. M.; Brouwers, J. F.; Van De Lest, C. H. A.; Bertijn, I.; Kraneburg, L.; Vos, P. L. A. M.; Stout, T. A. E.; Gadella, B. M. Potential Health and Environmental Risks of Three-Dimensional Engineered Polymers. *Environ. Sci. Technol. Lett.* **2018**, *5*, 80−85.

(19) Sivashankar, S.; Agambayev, S.; Alamoudi, K.; Buttner, U.; Khashab, N.; Salama, K. N. Compatibility Analysis of 3D Printer Resin for Biological Applications. *Micro Nano Lett.* **2016**, *11*, 654−659.

(20) Hart, C.; Didier, C. M.; Sommerhage, F.; Rajaraman, S. Biocompatibility of Blank, Post-Processed and Coated 3D Printed Resin Structures with Electrogenic Cells. *Biosensors* **2020**, *10*, 152.

(21) Ronca, A.; Maiullari, F.; Milan, M.; Pace, V.; Gloria, A.; Rizzi, R.; De Santis, R.; Ambrosio, L. Surface Functionalization of Acrylic Based Photocrosslinkable Resin for 3D Printing Applications. *Bioact. Mater.* **2017**, *2*, 131−137.

(22) Kurzmann, C.; Janjić, K.; Shokoohi-Tabrizi, H.; Edelmayer, M.; Pensch, M.; Moritz, A.; Agis, H. Evaluation of Resins for Stereolithographic 3D-Printed Surgical Guides: The Response of L929 Cells and Human Gingival Fibroblasts. *BioMed Res. Int.* **2017**, *2017*, 1−11.

(23) Inoue, Y.; Ikuta, K. Detoxification of the Photocurable Polymer by Heat Treatment for Microstereolithography. *Procedia CIRP* **2013**, *5*, 115−118.

(24) Popov, V. K.; Evseev, A. V.; Ivanov, A. L.; Roginski, V. V.; Volozhin, A. I.; Howdle, S. M. Laser Stereolithography and Supercritical Fluid Processing for Custom-Designed Implant Fabrication. *J. Mater. Sci.: Mater. Med.* **2004**, *15*, 123−128.

(25) Xu, Y.; Xepapadeas, A. B.; Koos, B.; Geis-Gerstorfer, J.; Li, P.; Spintzyk, S. Effect of Post-Rinsing Time on the Mechanical Strength and Cytotoxicity of a 3D Printed Orthodontic Splint Material. *Dent. Mater.* **2021**, *37*, e314−e327.

(26) Afshar-Mohajer, N.; Wu, C.-Y.; Ladun, T.; Rajon, D. A.; Huang, Y. Characterization of Particulate Matters and Total VOC Emissions from a Binder Jetting 3D Printer. *Build. Environ.* **2015**, *93*, 293−301.

(27) Gu, J.; Wensing, M.; Uhde, E.; Salthammer, T. Characterization of Particulate and Gaseous Pollutants Emitted during Operation of a Desktop 3D Printer. *Environ. Int.* **2019**, *123*, 476−485.

(28) Yi, J.; LeBouf, R. F.; Duling, M. G.; Nurkiewicz, T.; Chen, B. T.; Schwegler-Berry, D.; Virji, M. A.; Stefaniak, A. B. Emission of Particulate Matter from a Desktop Three-Dimensional (3D) Printer. *J. Toxicol. Environ. Health, Part A* **2016**, *79*, 453−465.

(29) Azimi, P.; Zhao, D.; Pouzet, C.; Crain, N. E.; Stephens, B. Emissions of Ultrafine Particles and Volatile Organic Compounds from Commercially Available Desktop Three-Dimensional Printers with Multiple Filaments. *Environ. Sci. Technol.* **2016**, *50*, 1260−1268.

(30) Stephens, B.; Azimi, P.; El Orch, Z.; Ramos, T. Ultrafine Particle Emissions from Desktop 3D Printers. *Atmos. Environ.* **2013**, *79*, 334−339.

(31) Unwin, J.; Coldwell, M. R.; Keen, C.; McAlinden, J. J. Airborne Emissions of Carcinogens and Respiratory Sensitizers during Thermal Processing of Plastics. *Ann. Occup. Hyg.* **2012**, *57*, 399−406.

(32) Väisänen, A. J. K.; Hyttinen, M.; Ylönen, S.; Alonen, L. Occupational Exposure to Gaseous and Particulate Contaminants Originating from Additive Manufacturing of Liquid, Powdered, and Filament Plastic Materials and Related Post-Processes. *J. Occup. Environ. Hyg.* **2019**, *16*, 258−271.

(33) *ISO 18562-1:2017(En), Biocompatibility Evaluation of Breathing Gas Pathways in Healthcare Applications—Part 1: Evaluation and Testing within a Risk Management Process*; International Organization for Standardization, 2017.

(34) Clarke, A. L.; Stephens, A. F.; Liao, S.; Byrne, T. J.; Gregory, S. D. Coping with COVID-19: Ventilator Splitting with Differential Driving Pressures Using Standard Hospital Equipment. *Anaesthesia* **2020**, *75*, 872−880.

(35) Koss, A.; Yuan, B.; Warneke, C.; Gilman, J. B.; Lerner, B. M.; Veres, P. R.; Peischl, J.; Eilerman, S.; Wild, R.; Brown, S. S.; Thompson, C. R.; Ryerson, T.; Hanisco, T.; Wolfe, G. M.; Clair, J. M. S.; Thayer, M.; Keutsch, F. N.; Murphy, S.; De Gouw, J. Observations of VOC Emissions and Photochemical Products over US Oil- and Gas-Producing Regions Using High-Resolution H3O+ CIMS (PTR-ToF-MS). *Atmos. Meas. Tech.* **2017**, *10*, 2941−2968.

(36) Neyman, G.; Irvin, C. B. A Single Ventilator for Multiple Simulated Patients to Meet Disaster Surge. *Acad. Emerg. Med.* **2006**, *13*, 1246−1249.

(37) Yuan, B.; Koss, A. R.; Warneke, C.; Coggon, M.; Sekimoto, K.; De Gouw, J. A. Proton-Transfer-Reaction Mass Spectrometry:

https://doi.org/10.1021/acsomega.1c04695
ACS Omega 2021, 6, 30726−30733

Applications in Atmospheric Sciences. *Chem. Rev.* **2017**, *117*, 13187−13229.
(38) Krechmer, J.; Lopez-Hilfiker, F.; Koss, A.; Hutterli, M.; Stoermer, C.; Deming, B.; Kimmel, J.; Warneke, C.; Holzinger, R.; Jayne, J.; Worsnop, D.; Fuhrer, K.; Gonin, M.; De Gouw, J. Evaluation of a New Reagent-Ion Source and Focusing Ion-Molecule Reactor for Use in Proton-Transfer-Reaction Mass Spectrometry. *Anal. Chem.* **2018**, *90*, 12011−12018.
(39) Liu, X.; Deming, B.; Pagonis, D.; Day, D. A.; Palm, B. B.; Talukdar, R.; Roberts, J. M.; Veres, P. R.; Krechmer, J. E.; Thornton, J. A.; de Gouw, J. A.; Ziemann, P. J.; Jimenez, J. L. Effects of Gas−Wall Interactions on Measurements of Semivolatile Compounds and Small Polar Molecules. *Atmos. Meas. Tech.* **2019**, *12*, 3137−3149.
(40) Riva, M.; Rantala, P.; Krechmer, J. E.; Peräkylä, O.; Zhang, Y.; Heikkinen, L.; Garmash, O.; Yan, C.; Kulmala, M.; Worsnop, D.; Ehn, M. Evaluating the Performance of Five Different Chemical Ionization Techniques for Detecting Gaseous Oxygenated Organic Species. *Atmos. Meas. Tech.* **2019**, *12*, 2403−2421.
(41) Cappellin, L.; Karl, T.; Probst, M.; Ismailova, O.; Winkler, P. M.; Soukoulis, C.; Aprea, E.; Märk, T. D.; Gasperi, F.; Biasioli, F. On Quantitative Determination of Volatile Organic Compound Concentrations Using Proton Transfer Reaction Time-of-Flight Mass Spectrometry. *Environ. Sci. Technol.* **2012**, *46*, 2283−2290.
(42) Sekimoto, K.; Li, S.-M.; Yuan, B.; Koss, A.; Coggon, M.; Warneke, C.; de Gouw, J. Calculation of the Sensitivity of Proton-Transfer-Reaction Mass Spectrometry (PTR-MS) for Organic Trace Gases Using Molecular Properties. *Int. J. Mass Spectrom.* **2017**, *421*, 71−94.
(43) McManus, J. B.; Zahniser, M. S.; Nelson, D. D. Dual Quantum Cascade Laser Trace Gas Instrument with Astigmatic Herriott Cell at High Pass Number. *Appl. Opt.* **2011**, *50*, A74.
(44) Herndon, S.; Zahniser, M. S.; Nelson, D. D.; Shorter, J.; McManus, J. B.; Jiménez, R.; Warneke, C.; de Gouw, J. A. Airborne Measurements of HCHO and HCOOH during the New England Air Quality Study 2004 Using a Pulsed Quantum Cascade Laser Spectrometer. *J. Geophys. Res.: Atmos.* **2007**, *112*, D10S03.
(45) Krechmer, J. E.; Pagonis, D.; Ziemann, P. J.; Jimenez, J. L. Quantification of Gas-Wall Partitioning in Teflon Environmental Chambers Using Rapid Bursts of Low-Volatility Oxidized Species Generated in Situ. *Environ. Sci. Technol.* **2016**, *50*, 5757−5765.
(46) Pagonis, D.; Krechmer, J. E.; de Gouw, J.; Jimenez, J. L.; Ziemann, P. J. Effects of Gas−Wall Partitioning in Teflon Tubing and Instrumentation on Time-Resolved Measurements of Gas-Phase Organic Compounds. *Atmos. Meas. Tech.* **2017**, *10*, 4687−4696.

https://doi.org/10.1021/acsomega.1c04695
ACS Omega 2021, 6, 30726−30733